

1    **Supplementary Material:**

2

3    **M1. Quality assessment**

4

5    Subjects with corrupted raw MRI data (n=4 patients) were excluded from the analysis. The  
6    image quality of resting-state MRI scans was assessed by visual inspection of the temporal  
7    signal-to-noise ratio (tSNR) distribution and mean time series across slices. Subjects displaying  
8    EPI distortion effect (n=1 control) were excluded from the analysis. Functional images  
9    exhibiting high degree of head framewise displacement (FD > 1 mm) in more than 15 volumes  
10   were discarded (n=1 patient) (Power et al., 2012). Based on the mean FD-value distribution  
11   across all scans, images with a mean head displacement exceeding 3.5 mm were excluded (n=1  
12   control, n=5 patients). The impact of the motion control was demonstrated with whole-brain  
13   signal measures before and after motion correction. This included measuring the mean square  
14   root of differentiated time series of each voxel and the global BOLD signal (Power et al., 2014).  
15   Image co-registration quality was visually inspected with the FreeSurfer's automated white  
16   matter contours and mean functional image overlays. In cases of poor alignment between white  
17   matter contours and mean EPI images, subjects were excluded from further analysis (n=1  
18   control). The source code for the automated quality assessment pipeline is available at  
19   <https://github.com/sheyma/mriqc/tree/master>, and an example of a quality assessment report at  
20   [https://github.com/sheyma/mriqc/blob/master/mriqc/examples/sd02\\_day1.pdf](https://github.com/sheyma/mriqc/blob/master/mriqc/examples/sd02_day1.pdf).

21

ID	vascular stroke territory	age	sex	lesion volume (cm <sup>3</sup> )	scan days post-stroke	NIHSS admission	NIHSS discharge	r <sub>s</sub> (G1)	r <sub>s</sub> (G2)	r <sub>s</sub> (G3)
sd02	L, AchA	47	m	5.18	days 0, 1, 5	6	1	0.16	-0.28	0.27
sd05	L, MCA	51	m	7.48	days 0, 1, 5	5	3	0.14	-0.06	0.30
sd08	L, MCA	64	m	4.08	days 0, 1, 5	1	0	-0.06	0.15	-0.13
sd10	L, MCA	67	f	3.65	days 0, 1, 5	0	0	-0.01	0.04	0.09
sd13	R, MCA	76	m	1.86	days 0, 1, 5	7	0	0.04	-0.03	0.17
sd14	L, MCA	72	f	1.22	days 0, 1, 5	0	0	0.11	-0.13	0.15
sd16	R, MCA	54	m	2.03	days 0, 1, 5	1	0	-0.19	0.13	0.11
sd17	L, PCA	43	m	2.11	days 0, 1, 5	3	2	0.09	0.39	0.07
sd21	R, MCA	72	f	14.09	days 0, 1, 5	1	0	0.07	0.09	0.18
sd25	L, PCA	71	f	6.80	days 0, 1, 5	5	0	0.10	0.12	0.18
sd26	L, PCA	79	m	3.19	days 0, 1, 5	2	-	0.14	-0.04	0.16
sd28	R, PCA	73	f	3.38	days 0, 1, 5	5	2	0.32	-0.17	0.22
sd31	R, PCA	81	f	3.21	days 0, 1, 5	4	2	0.17	-0.10	0.21
sd32	L, MCA	47	m	2.51	days 0, 1, 5	11	0	-0.06	-0.30	0.01
sd33	L, PCA	68	m	4.37	days 0, 1, 5	1	1	0.34	0.16	0.13
sd35	L, MCA	75	f	7.26	days 0, 1, 5	3	2	0.25	0.03	0.22
sd36	L, MCA	50	m	2.27	days 0, 1, 5	1	1	0.27	-0.14	0.32
sd38	R, PCA	53	m	1.46	days 0, 1, 6	1	0	0.02	0.12	0.22
sd39	L, PCA	59	m	4.75	days 0, 1, 5	1	1	0.02	0.09	0.15
sd40	R, PCA	90	f	7.61	days 0, 1, 5	6	2	0.01	0.20	-0.01
sd42	R, MCA	72	m	3.89	days 0, 1, 5	0	0	-0.11	-0.13	0.09
sd43	R, AchA	75	f	2.51	days 0, 1, 5	4	4	0.13	0.01	0.13
sd44	R, MCA	78	m	3.43	days 0, 1, 5	1	2	0.17	-0.14	0.23
sd45	L, MCA	37	f	1.78	days 0, 1, 4	0	0	-0.22	-0.22	-0.23
sd46	L, MCA	63	f	5.43	days 0, 1, 4	1	2	0.18	-0.05	0.25
sd48	L, PCA	60	m	0.73	days 0, 1, 4	1	1	0.16	-0.17	0.14
sd49	R, PCA	63	m	6.75	days 0, 1, 5	1	1	0.11	0.10	0.11
sd52	R, MCA	81	m	2.13	days 0, 1, 5	0	0	0.25	0.17	0.22
<b>Mean</b>		65.04		4.11		2.57	1.00	0.09	-0.01	0.14
<b>std</b>		13.27		2.80		2.70	1.09	0.14	0.16	0.12

22

23 **Supplementary Table 1: Patient characteristics and statistical results.**

24 Abbreviations: AChA indicates Anterior Choroidal Artery; PCA, Posterior Cerebral Artery;  
 25 MCA, Middle Cerebral Artery; L, left; R, right; B, bilateral; f, female; m, male. NIHSS  
 26 (National Institute of Health Stroke Scale) scores were obtained at patient admission and  
 27 discharge days, r<sub>s</sub>: Spearman's rank-order correlation coefficient between concordance and  
 28 distance-to-lesion maps along Gradient 1 (G1), Gradient 2 (G2) and Gradient 3 (G3).

29

30

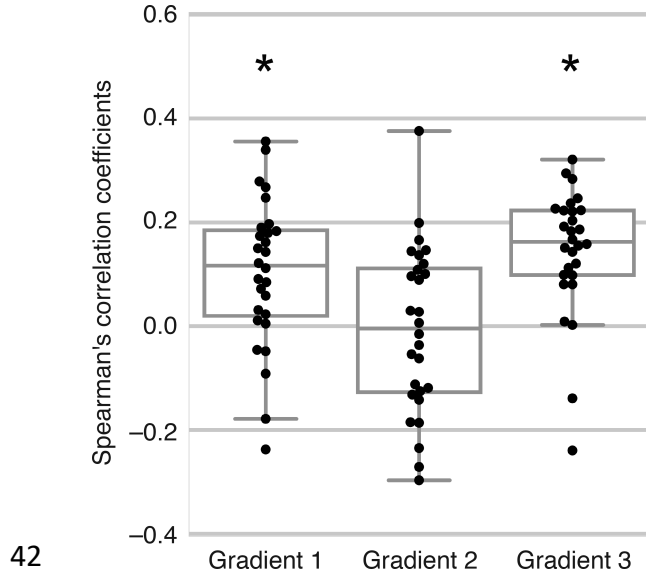
31 **M2. Controlling for variation in the mask size**

32 Since the grey matter masks used for the patients were computed at the individual level, they  
 33 varied slightly among patients (mask size range: 32,659 - 33,212 voxels). In order to make sure  
 34 this variation had no influence on our main result, we repeated the analysis using a common  
 35 mask (containing 30,314 voxels prior to lesion removal).

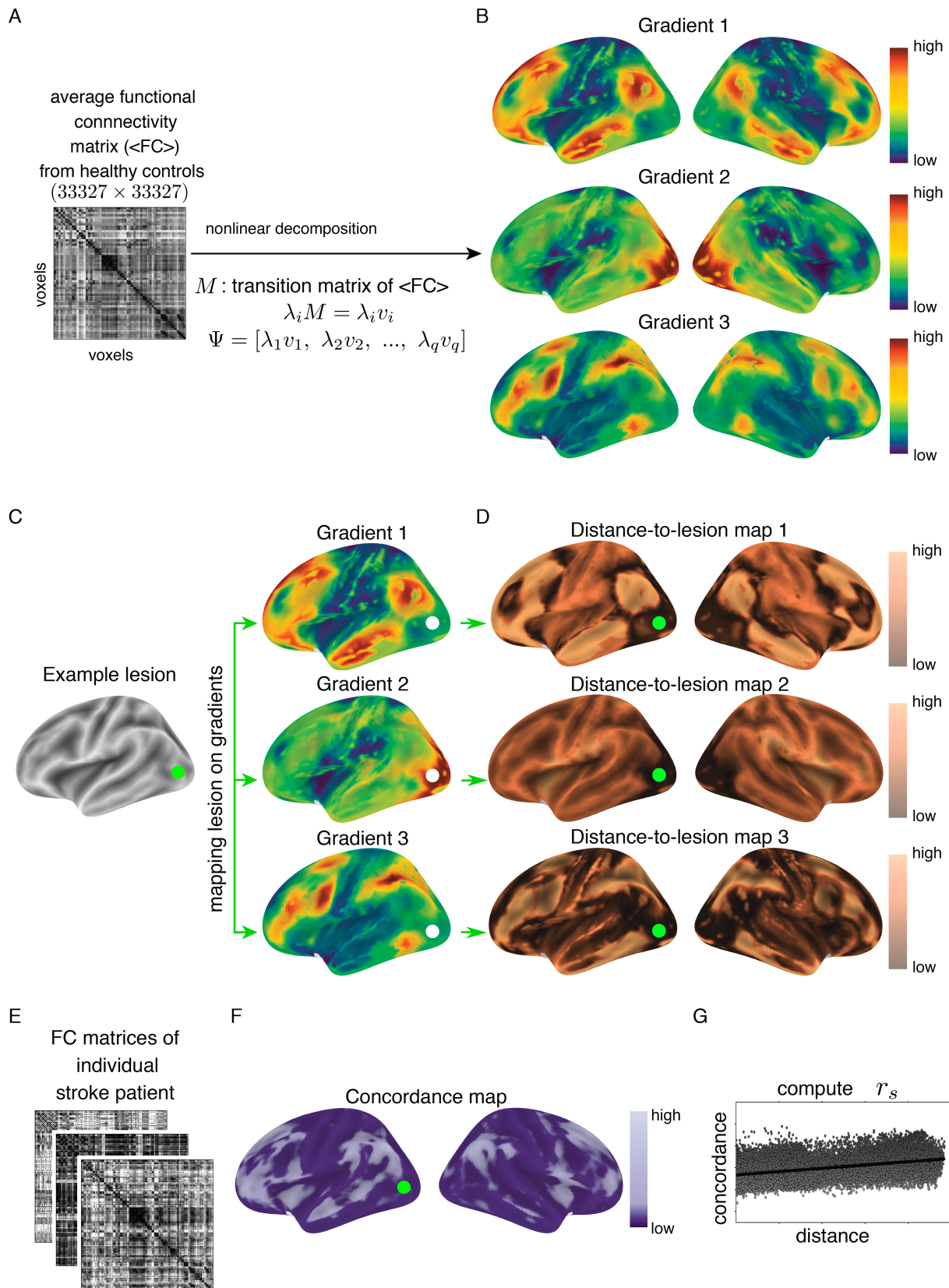
36 An averaged whole-brain resting-state mask was obtained across all stroke patients and scan  
 37 time points. This mask was multiplied with the grey matter template of healthy controls,

38 resulting in a new grey matter template of 30,134 voxels. The dilated lesions were excluded  
39 from the group-level grey matter template for individual patients. Using this more restricted  
40 grey matter template had no influence on the main result (Supplementary Figure S1).

41



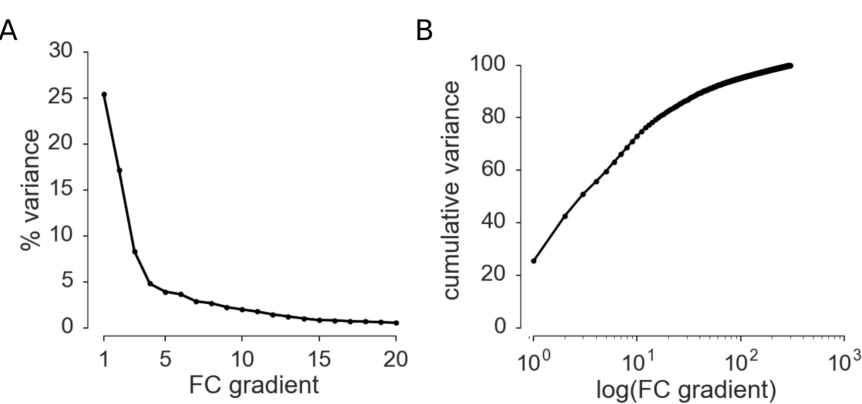
42  
43 **Supplementary Figure S1: Control analysis to overcome voxel number variation across**  
44 **patient's specific grey matter masks.** Our main result is replicated using a common grey  
45 matter template that was obtained across all stroke patients and resting-state sessions.  
46 Correlations were significantly positive for Gradient 1 ( $P=0.0015$ ,  $W=63.0$ , one-tailed  
47 Wilcoxon signed-rank test) and Gradient 3 ( $P=0.0001$ ,  $W=33.0$ ), but not for Gradient 2 ( $P=0.76$ ,  
48  $W=189.0$ ). Median correlations are  $\tilde{r}=0.12$  for Gradient 1,  $\tilde{r}=0.00$  for Gradient 2, and  $\tilde{r}=0.16$  for  
49 Gradient 3.  
50



51  
52

53 **Supplementary Figure S2: A detailed description of the analysis pipeline.** (A) A schematic  
54 illustration of averaged voxelwise functional connectivity matrix ( $\langle FC \rangle$ ) based on resting-state  
55 fMRI data of healthy subjects ( $n=28$ ). (B) Applying a nonlinear decomposition analysis on  
56 healthy controls data reveals first three connectivity gradients. (C) Anatomical lesion locations  
57 were delineated for individual patients and located along gradients. (D) The distance from each

58 voxel and the lesioned site was computed to create a voxelwise distance-to-lesion map for each  
 59 gradient. Distance-to-lesion is the subtraction of embedding values between each voxel and the  
 60 mean lesioned voxels. Voxels with lower values on the distance map (dark copper) shared  
 61 similar functional connectivity patterns with the lesioned site as characterized in healthy  
 62 controls. (E) For each patient, voxelwise functional connectivity (FC) matrices were computed  
 63 for the three resting-state fMRI scans post-stroke. (F) Connectivity concordance correlation  
 64 coefficient was used to quantify changes in functional connectivity patterns over time. Lower  
 65 concordance values (dark purple) reflect a larger change in functional connectivity patterns over  
 66 time. (G) For each gradient and each individual patient, the relationship between the distance-  
 67 to-lesion and concordance values was tested using Spearman's rank-order correlation  
 68 coefficient ( $r_s$ ) at the voxelwise level. The lesioned voxels were excluded from this analysis to  
 69 capture indirect, rather than local effects of the lesion.  
 70



71  
 72 **Supplementary Figure S3: Variance explained by connectivity gradients based on**  
 73 **nonlinear decomposition of functional connectivity data from healthy controls (n=28).** The  
 74 variance percentage (y-axis, A) explained by the first 20 gradients (x-axis, A) and the  
 75 cumulative variance (y-axis, B) carried by the first 300 gradients (x-axis, B) are depicted. The  
 76 variance drops exponentially with increasing number of gradients. The first three gradients used  
 77 for the current analysis account for 50.84 % of the total variance.  
 78

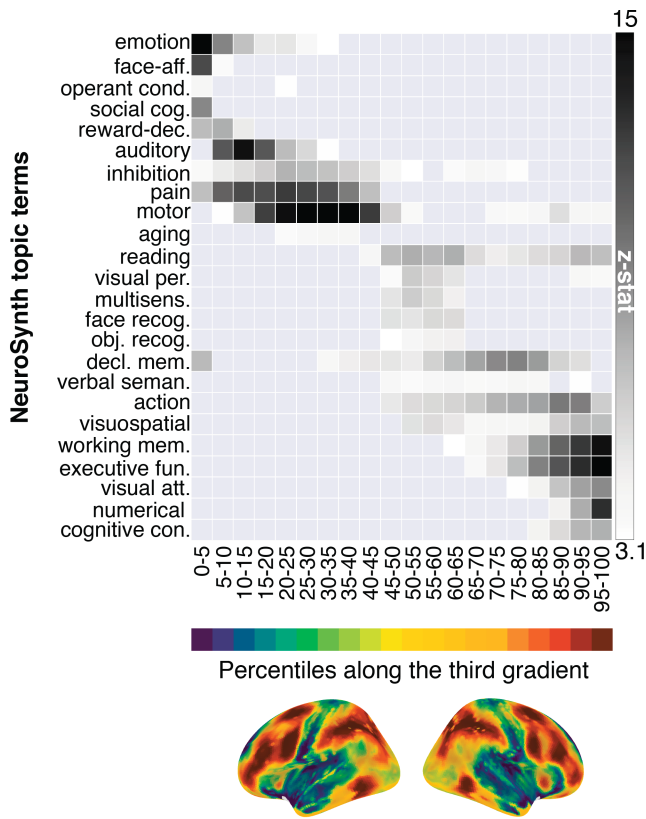
### 80 M3. The distribution of cognitive functions along connectivity gradients

81 Previous studies have demonstrated the cognitive dissociation captured along Gradient 1  
 82 (Margulies et al., 2016). However, this descriptive relationship has not been shown for Gradient  
 83 3. We therefore conducted a meta-analysis using the NeuroSynth database (Yarkoni et al.,  
 84 2011) to assess the topic terms associated with location along Gradient 3. Analysis followed a  
 85 previously published procedure (Margulies et al., 2016), and included 24 topic terms (Figure  
 86 S4). The volumetric map of Gradient 3 was divided into bins of five percentile size, creating  
 87 20 maps/regions-of-interest ranging from 0-5% to 95-100%. Each of the 20 maps was then  
 88 binarized and fed as an input to the meta-analysis. The output of the analysis was a z-statistic  
 89 associated with the feature term for each given map. The terms were ordered based on the  
 90 weighted mean for visualization.

91 This descriptive analysis supports the functional dissociation of transmodal (i.e., default-mode  
 92 network, DMN) and unimodal areas from multi-modal regions as captured along Gradient 3.

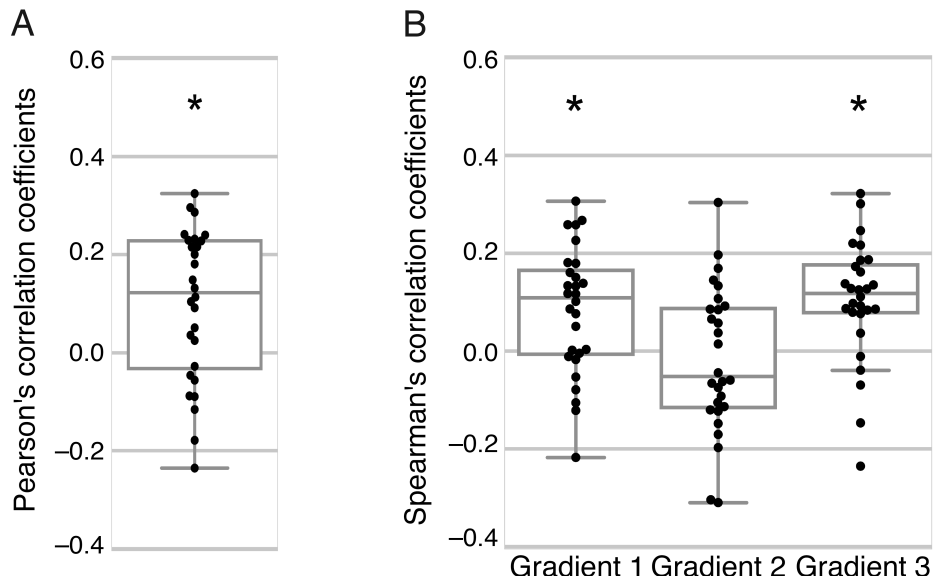
93 Topic terms such as ‘social cognition’ associated with DMN activation are situated at the far  
 94 end of the gradient, followed by unimodal areas associated with topic terms such as ‘auditory’  
 95 and ‘motor’. At the other extreme of the gradient, topic terms such as ‘visuospatial’ and  
 96 ‘working memory’ are associated with areas of the attention and memory domains.

97



98

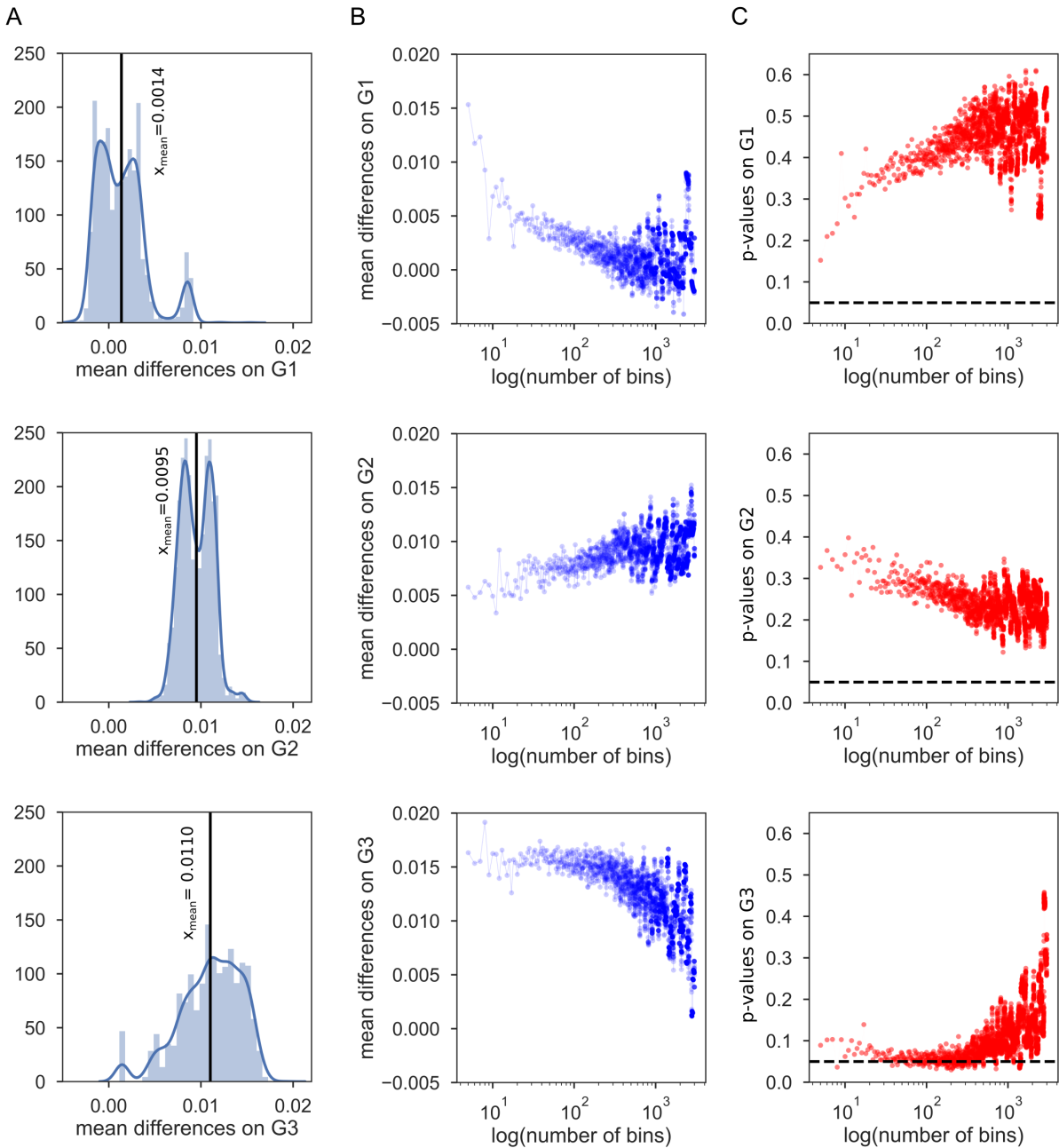
99 **Supplementary Figure S4: NeuroSynth meta-analysis of regions of interest along**  
 100 **Gradient 3 using 24 topic terms.** The gradient is divided into 20 bins of equal size each  
 101 representing five percentiles (blue-to-red colorbar and corresponding spatial map of the  
 102 gradient). The z-statistic (grey colorbar) represents the association with a topic term for a given  
 103 map. Topic terms are ordered by the weighted mean of their location along the gradient. High-  
 104 order abstract terms associated with default-mode network at the top are followed by sensory  
 105 processing terms, and then at the far end memory and attention related processes.  
 106 Abbreviations: face-aff.: face-affective processing; operant cond.: operant conditioning; social  
 107 cond.: social conditioning; reward-dec.: reward-based decision making; auditory: auditory  
 108 processing; visual per.: visual perception; multisens.: multisensory processing; face recog.:  
 109 face recognition; obj. recog.: object recognition; decl. mem.: declarative memory; verbal  
 110 seman.: verbal semantics; working mem.: working memory, executive fun.: executive function,  
 111 visual att.: visual attention; numerical: numerical cognition; cognitive con.: cognitive control.  
 112



113  
114  
115

116 **Supplementary Figure S5: The influence of anatomical lesion location on functional**  
 117 **connectivity changes.** (A) Box plot indicates the distribution of Pearson's correlation  
 118 coefficients for individual patients (y-axis) representing the relationship between distance from  
 119 the lesion in anatomical space and changes in functional connectivity over time. A positive  
 120 correlation indicates that voxels situated nearby the stroke lesion have a higher alteration in  
 121 their functional connectivity patterns. One-tailed Wilcoxon signed-rank test shows a significant  
 122 positive correlation at the group level ( $\tilde{r}=0.12$ ,  $P=0.0042$ ,  $W=77.0$ ). Functional connectivity  
 123 alters at a higher degree for voxels that are anatomically closer to the lesion. (B) Box plots  
 124 represent the distribution of Spearman's rank-order correlation coefficients from individual  
 125 patients (y-axis) for three main gradients, respectively (x-axis) following the regression of  
 126 anatomical distance as a covariate of no interest. A positive correlation reflects a significant  
 127 relationship between changes in functional connectivity and location on respective connectivity  
 128 gradients independent of the anatomical lesion location. The relationship between location  
 129 along connectivity gradients and functional connectivity changes remains unchanged for all  
 130 three gradients (one-tailed Wilcoxon signed-rank test, Gradient 1:  $\tilde{r}=0.11$ ,  $P=0.0046$ ,  $W=78.0$ ,  
 131 Gradient 2:  $\tilde{r}=-0.05$ ,  $P=0.50$ ,  $W=173.0$ , Gradient 3:  $\tilde{r}=0.12$ ,  $P=0.0006$ ,  $W=51.0$ ).

132  
133  
134



135

136

137 **Supplementary Figure S6: Relationship between the clinical trajectory and overall delta-**  
 138 **concordance measure detected along individual gradients.** (A) Distribution of the difference  
 139 in mean delta-concordance ( $\Delta CCC$ ) between patient groups (“clinically-changed” versus “no  
 140 clinical change”) across varying bin numbers (from 5 to 3000) are plotted for individual  
 141 gradients (Gradient 1, top; Gradient 2, middle; Gradient 3, bottom).  $\Delta CCC$  scores depict the  
 142 spatial concordance differences in lesion-unaffected and lesion-affected bins of a gradient. The  
 143 difference in mean  $\Delta CCC$  between patient groups was computed for each of the bin numbers  
 144 used to parcellate the connectivity gradient into parcels of equal size. A positive difference  
 145 suggests that the group of patients who changed their clinical score over the first week  
 146 demonstrated a higher degree of change in functional connectivity in affected portions of the  
 147 gradient. We found no significant difference between the groups across varying bin numbers  
 148 following False Discovery Rate (FDR) correction (threshold = 0.1, number of tests = 2996).  
 149 Values are centered around zero for Gradient 1, however, they are positively distributed for

150 Gradient 2 and Gradient 3. (B) The mean difference in  $\Delta CCC$  between patient groups (y-axis)  
151 depicted for each bin number (x-axis). (C) The corresponding p-values (y-axis) for each bin  
152 number (x-axis) obtained following group comparison using a permutation test. The dashed  
153 black line represents  $p = 0.05$ .

154

## References:

- 155 Margulies, D.S., Ghosh, S.S., Goulas, A., Falkiewicz, M., Huntenburg, J.M., Langs, G.,  
156 Bezgin, G., Eickhoff, S.B., Castellanos, F.X., Petrides, M., Jefferies, E., Smallwood, J.,  
157 2016. Situating the default-mode network along a principal gradient of macroscale  
158 cortical organization. Proc. Natl. Acad. Sci. 113, 12574–12579.  
159 <https://doi.org/10.1073/pnas.1608282113>
- 160 Power, J.D., Barnes, K.A., Snyder, A.Z., Schlaggar, B.L., Petersen, S.E., 2012. Spurious but  
161 systematic correlations in functional connectivity MRI networks arise from subject  
162 motion. Neuroimage 59, 2142–2154. <https://doi.org/10.1016/j.neuroimage.2011.10.018>
- 163 Power, J.D., Mitra, A., Laumann, T.O., Snyder, A.Z., Schlaggar, B.L., Petersen, S.E., 2014.  
164 Methods to detect, characterize, and remove motion artifact in resting state fMRI.  
165 Neuroimage 84, 320–341. <https://doi.org/10.1016/j.neuroimage.2013.08.048>
- 166 Yarkoni, T., Poldrack, R.A., Nichols, T.E., Van Essen, D.C., Wager, T.D., 2011. Large-scale  
167 automated synthesis of human functional neuroimaging data. Nat. Methods 8, 665–670.  
168 <https://doi.org/10.1038/nmeth.1635>